# Volcanic Eruption Observations from an Elevated Point of Stromboli Using Thermal Infrared Hyperspectral Imaging

Many urban areas are located near active volcanoes around the world. Therefore, scientific research on different indicators of imminent eruptions is carried out on an ongoing basis. Due to the hazardous and unpredictable behavior of volcanoes, remote sensing technologies are normally preferred for investigations. Over the years, the Telops Hyper-Cam, a high-performance infrared hyperspectral camera, has established itself as a reference tool for investigating gas clouds over large distances. In order to illustrate the benefits of standoff infrared hyperspectral imaging for characterizing volcanic processes, many different measurements were carried out from an elevated point (~800 m) of the Stromboli volcano (Italy) by researchers from the *Université Blaise-Pascal* (Clermont-Ferrand, France). The Stromboli volcano is well known for its periodic eruptions of small magnitude containing various proportions of ash, lava and gases. Imaging was carried out at a relatively high spectral and spatial resolution before and during eruptions from the North-East crater. Both sulfur dioxide ($SO_2$) and sulfur tetrafluoride ($SiF_4$) could be successfully identified within the volcano's plume from their distinct spectral features. Quantitative chemical maps for both gases are presented in this work. The results show that standoff thermal infrared hyperspectral imaging provides unique insights for a better understanding of volcanic eruptions.

## Introduction

Volcanic soils are among the richest agricultural farmlands on Earth. For this reason, many populations have established themselves close to active volcanoes over the years. Therefore, finding reliable indicators of imminent eruptions is a matter of civil security. Research activities on volcanoes are very challenging due to their unpredictable behavior and the life-threathening situations they may create. Volcanic emissions contain great proportions of water vapor ($H_2O$) and carbon dioxide ($CO_2$). Depending on the type of volcano, emissions may contain variable proportions of toxic/corrosive gases such as sulfur dioxide ($SO_2$), hydrogen chloride (HCl), hydrogen fluoride (HF) and silicon tetrafluoride ($SiF_4$). Ash is also omnipresent in volcanic emissions. During volvanic eruptions, lava (molten rock) and ash are expelled in the atmosphere at high velocity by hot gases under high pressure. Since these circomstances represent destructive conditions for most scientific instruments, sampling techniques and close-range analysis are not viable avenues. Therefore, investigations using remote sensing techniques like $SO_2$ UV imaging and infrared imaging (Figure 1) provide considerable benefits for the researchers.

**Figure 1 Volcanic eruption investigation carried out with the Telops Hyper-Cam.**

Broadband thermal infrared imaging has been extensively used for characterizing volcanic environments in the past. However, only limited information can be obtained when investigating volcanic gases using this technique. The spectral emissivity properties of the great majority of gases found in volcanic plumes is incompatible with the conventional broadband infrared imaging approach. Each gas typically absorbs and emits infrared radiation over a very narrow spectral range (approximately tenths of microns), with a a very unique pattern, when compared with the whole infrared FPA detector sensitivity range. Therefore, it is not possible to distinguish nor quantify gases due to the lack of spectral information; broadband thermal imaging thus essentially provides qualitative results in such a case. Open-path FT-IR was shown to provide interesting information about the chemical content of vents and fumerols [1,2]. However, the lack of spatial information and the geometrical constraints of this technique limits its applicability. The use of passive single-pixel FT-IR scanning systems for investigating volcanic emissions was also previously reported [3,4]. However, the time required for scanning the whole volcano's plume area somewhat limits the use of this approach to steady-state conditions, such as passive degassing. A comparative study between a UV camera and a thermal infrared hyperspectral imaging system for determining the $SO_2$ content of volcanic emission was recently published [5].

In order to investigate volcanoes under a highly dynamic context, researchers from the Université Blaise Pascal used a Telops Hyper-Cam, a standoff infrared hyperspectral imaging (HSI) camera, to characterize volcanic plumes from an elevated point (altitude of ~800 m) of the Stromboli volcano in Italy (Figure 2A, Rochette),. The Stromboli volcano is well known for its periodic eruptions of small magnitude containing various proportions of ash, lava and gases. The measurement location lied at an altitude similar to the North-East crater and at a line-of-sight distance of 400 m from it (Figure 2). Under these conditions, it was possible to characterize multiple eruptions over a period of 2 days. The selectivity provided by HSI allowed the identification of both $SO_2$ and $SiF_4$. Quantitative chemical maps were also obtained for both gases to track their presence before, during and after an eruption. The results illustratre how the combined spatial, spectral and temporal resolution of the Telops Hyper-Cam can provide unique insights into the characterization of volcanic eruptions.

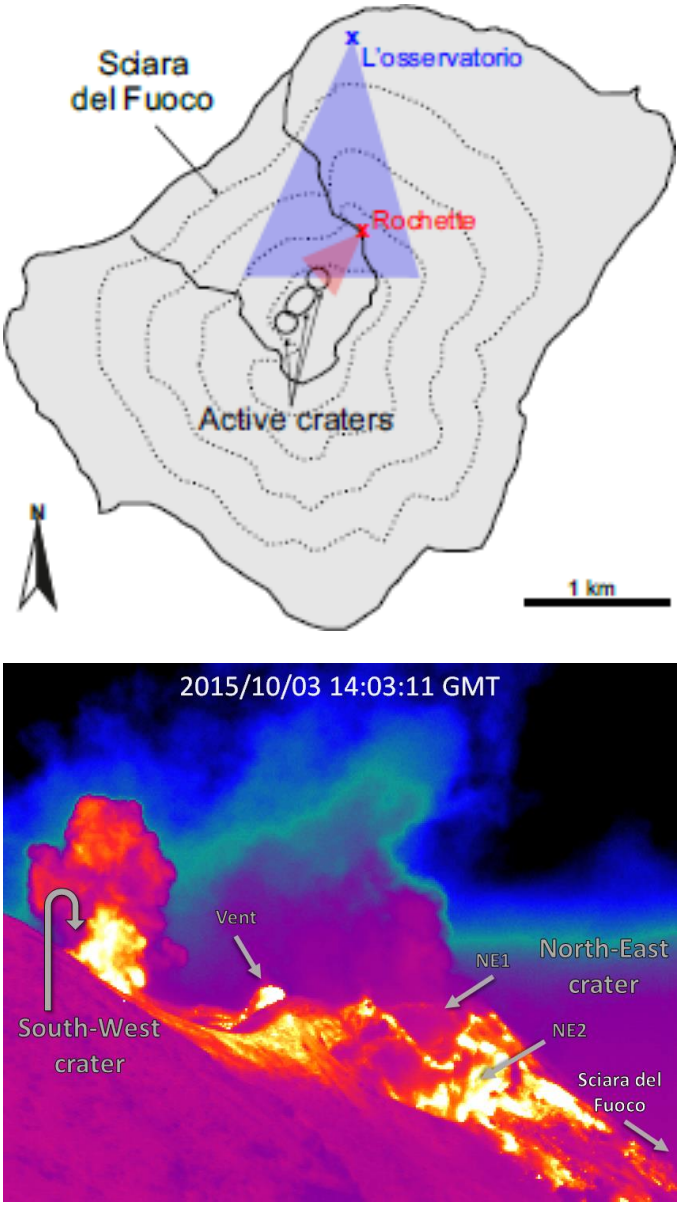


**Figure 2 Topographic map of the Stromboli volcano (top) [5]. Results presented in this work are from measurements carried out at the Rochette location. Broadband infrared image overview of the Stromboli craters as seen from the Rochette location (bottom). The image was captured during an eruption of the South-West crater.**

## Experimental Information

### The Telops Hyper-Cam

The Telops Hyper-Cam LW is a lightweight and compact hyperspectral imaging instrument that uses Fourier transform infrared (FTIR) technology. The Hyper-Cam LW features a closed-cycle stirling-cooled mercury-cadmium-telluride (MCT) focal plane array (FPA) detector, which contains 320×256 pixels over a basic 6.4°×5.1° field of view (FOV). The spectral resolution is user-selectable up to 0.25 $cm^{-1}$ over the 7.7 to 11.8 µm (875 – 1315 $cm^{-1}$) spectral range. A 0.25× wide-angle demagnifying telescope was used for the measurements, leading to a FOV of 25.6°×20.4°. The sensor was located at the Rochetta shelter, lying at an altitude of approximately 800 m, and from an approximately 400-m line of sight distance from the North-East crater. The distance was determined from a laser rangefinder measurement. Under these conditions, the effective pixel size was about 200 $cm^2$/pixel. Measurement sequences were carried out in various acquisition conditions. For the monitoring of eruptions, the instrument's FOV was narrowed down to 200×200 pixels, and the spectral resolution set to 8 $cm^{-1}$ (70 spectral bands), leading to an effective scan rate of 3 sec/hypercube. To characterize the volcanic emission content, the instrument's FOV was narrowed down to 64×64 pixels, and the spectral resolution set to 1 $cm^{-1}$ (525 spectral bands). Outside temperature and relative humidity ranged from 15 to 22 °C and from 30 to 50 % respectively during the different experiments.

### Data Preprocessing

The Telops Hyper-Cam uses FT-IR technology with which full-frame images are captured for each optical path difference (OPD) mirror position of the Michelson interforemoter at a high velocity. This time-domain data is then converted into a hyperspectral cube, i.e. frequency-domain data, after performing fast Fourier transform (FFT). However, the high-temperature moving particles produced by volcanic eruptions lead to artefacts in the time-domain data, which result in additional frequencies in the spectra after FFT. In order to recover the information contained in these pixels, the erratic signal modulations associated with these hot and moving particles were blanked and/or discarded. The FFT of such recovered interferograms then resulted in spectra with lower effective spectral resolution.

### Radiative Transfer Model

The broadband images associated with the hyperspectral data were obtained by summing, for each pixel, the radiance measured at each wavenumber over the whole FPA detector spectral range. Column density results were obtained by solving Equation 1, where $L$ is the measured radiance at sensor, $L_{bkg}$, the radiance at the back of the gas plume, $\varepsilon_{bkg}$, the spectral emissivity associated with the background, $Dw$, the downwelling radiance, $\tau_{plume}$, the gas plume transmittance, $L_{plume}$, the self-emission radiance associated with the gas plume, and $L_{atm}$ and $\tau_{atm}$, the self-emission radiance and transmittance associated with the atmosphere respectively.

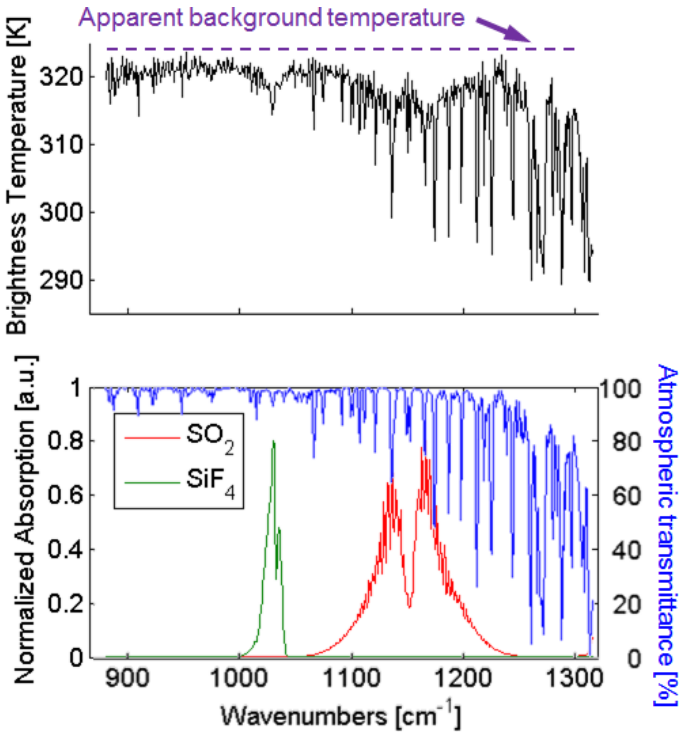


**Figure 3 High-resolution spectrum of pixel located deep within NE2 crater (top). The estimated atmospheric transmittance (blue curve), $SO_2$ (red curve) and $SiF_4$ (green curve) reference spectra are also presented (bottom).**

Self-emission is function of the object's thermodynamic temperature while transmittance is function of gas concentration (expressed in ppm), path length $l$ (expressed in meters), and the gas molar absorptivity $\kappa$, as expressed in Equation 2.

**Equation 1**

$$L = \left[\left(L_{bkg}\varepsilon_{bkg} + \left(1 - \varepsilon_{bkg}\right)Dw\right)\tau_{plume} + L_{plume}\left(1 - \tau_{plume}\right)\right]\tau_{atm} + L_{atm}(1 - \tau_{atm})$$

**Equation 2**

$$\tau_{plume} = \exp\left(-\sum \kappa l[gas]\right)$$

For the analysis, water vapor, sulfur dioxide, sulfur tetrafluoride and ash were used as gas plume components. The presence of ash is non-negligible in the gas plume and its impact on the gas plume transmittance was modeled as a featureless semi-translucent media. Even though direct quantification is not a straightforward procedure, an emissivity leading to a 10 % signal attenuation per km was attributed to the ash particles.

## Results and Discussion

Volcanic activity from all 3 craters (Central, South-West and North-East) of the Stromboli takes place on a regular basis. The elevated location near the Rochetta shelter provided a very good view of the North-East (NE) crater, as shown in Figure 1 and Figure 2. Eruption products from the South-West crater could be observed using both visible and infrared imaging, although no direct view of the crater was possible from the sensor location (see Figure 2). The central crater was located on the hillside and was likely out of sight from this location. Still, eruptions from both NE crater formations, i.e. NE1 and NE2, could be investigated using the HSI system. The sensor-to-crater distance was relatively close (about 400 m) compared with previous work [1-4], thus providing good spatial resolution and a detailed view of an eruption's sequence of events. The North-East crater is well known for its lava production falling into the famous Sciara del Fuoco. From an infrared-imaging perspective, this means that high-energy particles are traveling at a relatively high velocity within the imaging system field of view. These unsteady and dynamic scenes are somewhat incompatible with the acquisition mode of other open-path [1,2] and scanning [3,4] hyperspectral infrared sensors.

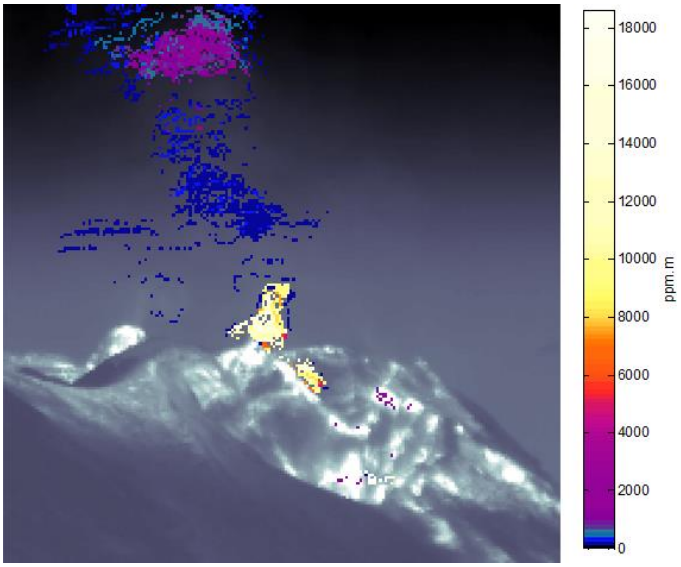


**Figure 4 $SO_2$ passive degassing from the North-East crater. The column density estimates are displayed over the broadband image for clarity purposes.**

### Passive Degassing

In order to evaluate the gas constitution of the volcanic emissions, a high spectral resolution hypercube was first recorded on an area corresponding to the deepest and hottest area of the NE2 crater. The recording was carried out between two eruptions in order to get representative data of a passive degassing phase. A representative spectrum from a single pixel of this hypercube is shown in Figure 3 (top), as well as a few reference spectra (Figure 3, bottom). The measured spectrum is shown on a brightness temperature scale in order to facilitate visualization and comparison with reference spectra plotted on an absorbance scale. The background, i.e. crater wall, behaves like a grey body (no spectral feature) of relatively high emissivity. The series of sharp absorption (downward) peaks result from absorption of the background self-emission ($L_{bkg}$) by the

atmospheric gases located in the sensor's line of sight (between the camera and the crater). The atmospheric absorption mostly results from $H_2O$, methane ($CH_4$) and nitrous oxide ($N_2O$) in the longwave infrared (LWIR) spectral range. In addition to common atmospheric components, absorption spectral features associated with $SO_2$ and $SiF_4$ can be distinguished within the measurement. $SO_2$ is a common gas found in volcanic emissions, while $SiF_4$ results from the reaction between HF and silicate minerals, such as quartz and pyroxene ($SiO_2$) from the rock walls, as shown in Equation 3.

**Equation 3**

$$SiO_2 + 4HF \rightarrow SiF_4 + 2H_2O$$

The presence of multiple gases of different chemical nature could be detected during the passive degassing phase. In the LWIR spectral range, $SO_2$ was among the dominant chemical species, after water vapor, in the volcanic emissions. A representative estimate of the $SO_2$ distribution during passive degassing is shown in Figure 4. During the measurement campaign, the NE1 crater was found to produce much more $SO_2$ than the NE2 crater. In Figure 4, it can be seen that the $SO_2$ column- density value was difficult to estimate near the crater's opening. This is mostly due to the presence of large amounts of aerosols (water droplets) and water vapor in this area. Water vapor is highly infrared-active and represents the major component of volcanic emissions. The hot water vapor produced by the volcano readily condensates as it cools down when reaching the atmosphere. All gases, including $SO_2$, undergo rapid cooling when exiting the volcano's environment. The presence of massive amounts of aerosol clouds create low thermal contrast conditions, which make infrared remote sensing impracticable under such circumstances. As the gas cloud mixture diffuses in the atmosphere, a gravity-driven separation of the aerosol-ash-gas mixture occurs. Since sky radiance normally creates high thermal contrast conditions, $SO_2$ ans $SiF_4$ can then more easily be detected and their contribution estimated. The effective depth of the volcanic plume is required, for each pixel, in order to convert column-density values into concentration values. As such values are unavailable with a single 2D sensor measurement, the conversion cannot be carried out easily. Nevertheless, it is possible to estimate the total amount of each gas in the camera's field of view knowing the distance between the Hyper-Cam and the crater as well as the optical configuration of the hyperspectral camera. For passive degassing, a total amount of 3.3 kg and 0.8 g of $SO_2$ and $SiF_4$ were estimated respectively.

## Stromboli Eruptions from the North-East Crater

The Stromboli volcano is well known for its regular eruptions of moderate amplitude. The content, i.e. relative proportion of ash, lava, $SO_2$ , $SiF_4$…., differs a lot from time to time. In order to illustrate the usefulness of passive thermal infrared HSI for the characterization of volcanic eruptions, two very different eruption sequences are presented. The first sequence from the NE1 crater contains large amount of $SO_2$ and lava bombs (see Figure 5), while the second sequence from the NE2 crater contains large amounts of ash and $SiF_4$ (see Figure 6). Because the two eruptions are of different nature, the column-density results are not presented on the same color scale. Nevertheless, the detailed investigation of these two sequences highlights the benefits and challenges associated with thermal infrared HSI of volcanic eruptions.

## Eruption Sequence from the NE1 Crater

The first investigated sequence corresponds to a violent eruption of the NE1 crater, as shown in Figure 5. Large amounts of ash and lava bombs were ejected during this eruption. Since lava is at a very high temperature, saturation of the infrared detector occurred due to the limited dynamic range of the instrument. Consequently, no signal processing could be carried out on these pixels. Still, quantitative chemical imaging of both $SO_2$ and $SiF_4$ could be carried out on the sequence. It is interesting to note the relative timing of the different events in Figure 5. Lava and ash first came out, likely propelled by a hot and high-pressure gas mixture rich in $SO_2$. The amount of $SO_2$ resulting from the eruption was much

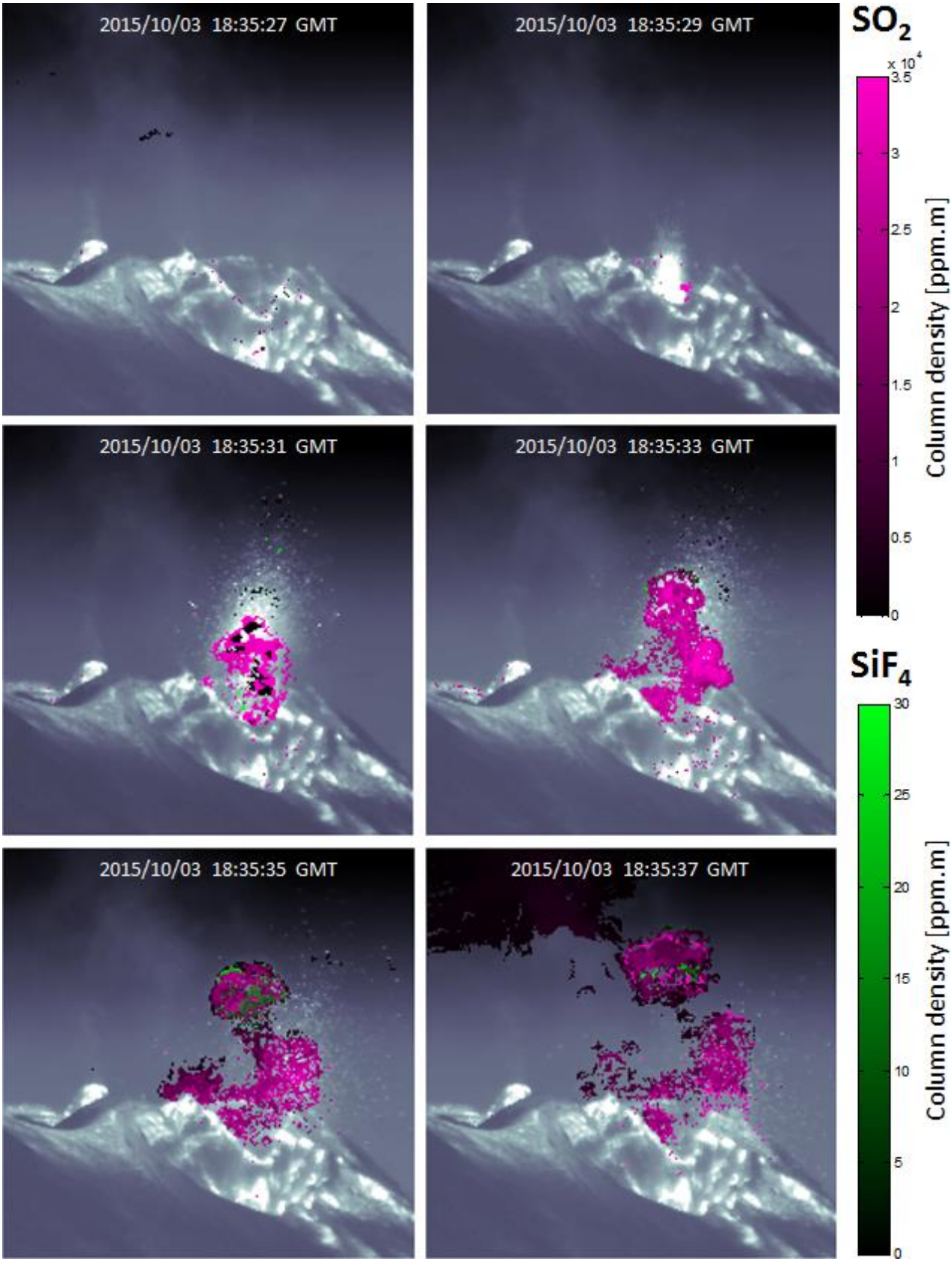


**Figure 5 Successive frames recorded during an eruption of the NE1 crater. The column-density results for $SO_2$ (purple) and $SiF_4$ (green), estimated from Equation 1, are displayed over the broadband image associated with each acquisition for clarity purposes.**

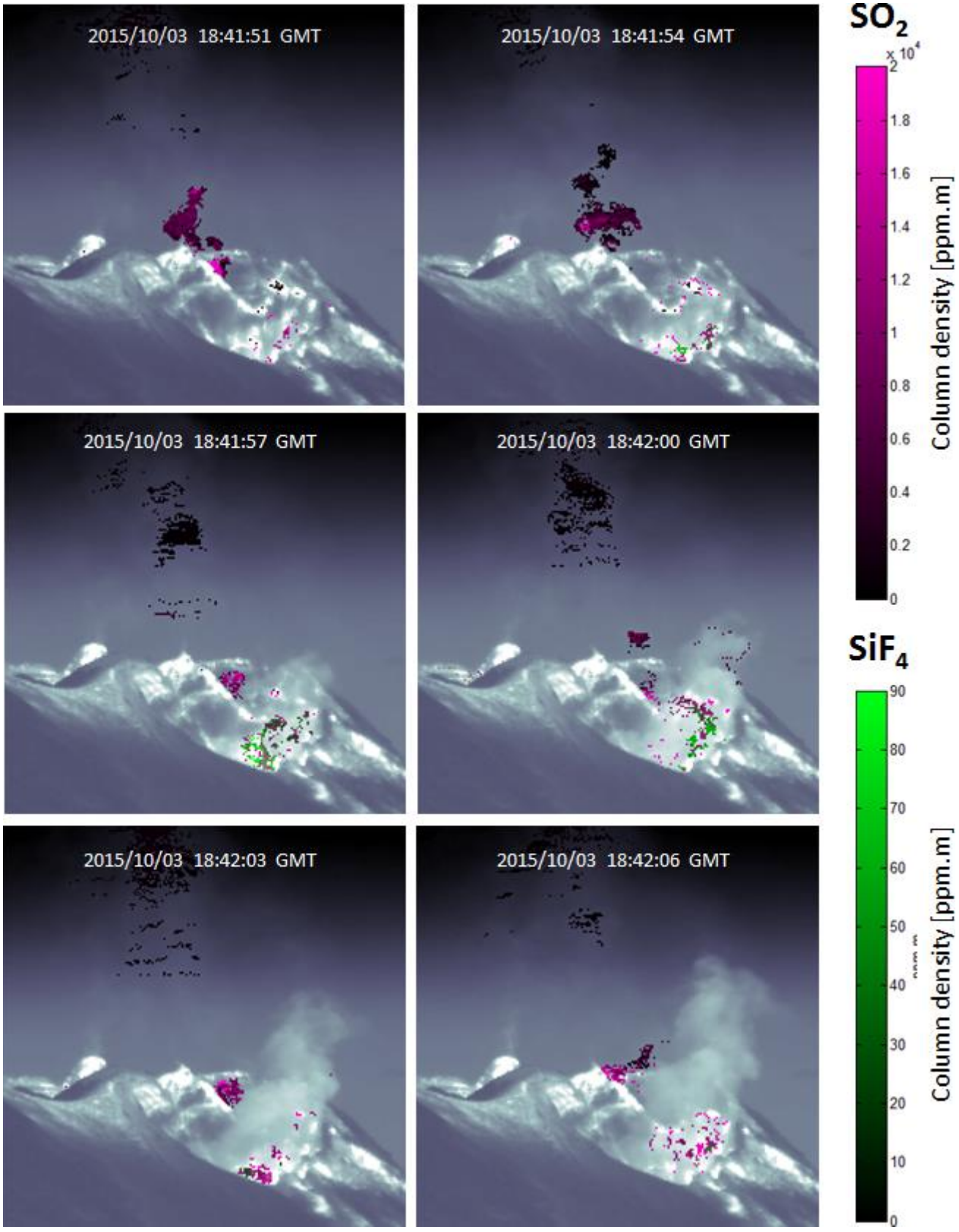


**Figure 6 Successive frames recorded during an eruption of the NE2 crater. The column-density results for $SO_2$ (purple) and $SiF_4$ (green), estimated from Equation 1, are displayed over the broadband image associated with each acquisition for clarity purposes.**

higher than the estimate carried out during a passive degassing phase (see Figure 4). The presence of $SiF_4$ could also be confirmed from its characteristic spectroscopic features in the hyperspectral data. Moreover, it appears that the $SiF_4$ gas cloud came out at a later stage as if $SiF_4$ was not fully mixed with the $SO_2$ gas cloud prior to the eruption. The fact that HF must first react with silicate minerals in order to produce $SiF_4$ might can explain this "kinetic" effect. As expected, the extent of the volcanic plume is much larger during an eruption than during the passive degassing stage. The total amount of $SO_2$ and $SiF_4$ found in the camera's field of view was estimated for the 4$^{th}$ frame presented in Figure 5 (2015/10/03 18:35:33 GMT) which was approximately captured during the mid-stage of the eruption process. Total amounts of 45 kg and 7 g were estimated for $SO_2$ and $SiF_4$ respectively. The estimated amount of $SO_2$ for a single eruption is in good agreement with previous work using a UV-$SO_2$ camera [7-8]. In both cases, these values are much larger that the amounts estimated during the passive degassing stage for both gases.

### Eruption Sequence from the NE2 Crater

The second investigated sequence corresponds to an eruption of relatively small magnitude of the NE2 crater, as shown in Figure 6. In this case, low amounts of ash and large amounts of water vapor were detected. The amount of $SO_2$ estimated in the emissions was higher than the amount observed during the passive degassing phase, but lower than the explosive eruption previously shown of the NE1 crater. On the other hand, the amount of $SiF_4$ resulting from this eruption sequence was significantly higher than what could be measured during passive degassing. For the same reasons expressed in the passive degassing phase, infrared remote sensing is very challenging in presence of large amounts of water vapor and aerosols. This might explain why relatively low amounts of $SO_2$ and $SiF_4$ could be detected in the emissions. The total amount of $SO_2$ and $SiF_4$ found in the camera's field of view was estimated for the 4$^{th}$ frame presented in Figure 6 (2015/10/03 18:41:57 GMT), which was again approximately captured during the mid-stage of the eruption process. Total amounts of 3 kg and 17 g were estimated for $SO_2$ and $SiF_4$ respectively. The amount of $SO_2$ produced by this eruption was found similar than the amount estimated during the passive degassing stage. However, the amount of $SiF_4$ was found much larger by a factor of 21.

**Figure 7 The stromboli ascension with the equipment.**

## Conclusion

For the first time, the North-East crater of the Stromboli volcano could be successfully investigated using passive thermal infrared hyperspectral imaging. Measurements carried out from an elevated point of the volcano allowed the characterization of the volcanic emissions resulting from passive degassing and moderate eruptions containing variable amounts of ash, lava, steam, $SO_2$ and $SiF_4$. In addition to obtaining spectroscopic confirmation of the presence of $SO_2$ and $SiF_4$, quantitative chemical imaging was carried out. The unpredictable nature of volcanic eruption illustrates the benefit of combined temporal, spectral and spatial resolution for imaging active volcanoes.

## Acknowledgments

Telops would like to acknowledge the support of Mathieu Gouhier and Jean-François Smekens from the Laboratoire Magmas et Volcans of the Université Blaise-

Pascale Clermont Ferrand, in France. Additional thanks to the rest of the crew for helping us to bring the equipment all the way to the top of the Stromboli volcano (Figure 7).

## References

[1] Francis, P., Chaffin, C., Maciejewski, A. and Oppenheimer, C. (1996): Remote determination of $SiF_4$ in volcanic plumes: A new tool for volcano monitoring, *Geophysical reaserach letters*, **23**(3), 249-252.

[2] Mori, T., Sato, M., Shimoike, Y. and Notsu, K. (2002): High $SiF_4$/HF ratio detected in Satsuma-Iwojima volcano's plume by remote FT-IR observation, *Earth Planets Space*, **54**, 249–256.

[3] Stremme, W., Krueger, A., Harig, R. and M. Grutter (2012): Volcanic $SO_2$ and $SiF_4$ visualization using 2-D thermal emission spectroscopy – Part 1: Slant-columns and their ratios, *Atmos. Meas. Tech.*, **5**, 275–288.

[4] Krueger, A., Stremme, W., Harig, R. and M. Grutter (2013): Volcanic $SO_2$ and $SiF_4$ visualization using 2-D thermal emission spectroscopy – Part 2: Wind propagation and emission rates, *Atmos. Meas. Tech.*, **6**, 47–61.

[5] Smekens, J-F. and Gouhier, M. (2015): Observation of passive and explosive emissions at Stromboli with a ground-based hyperspectral TIR camera, 2015 Fall Meeting, AGU, San Francisco, Abstract V51D-3056.

[6] Calvari, S., Intrieri, E., Di Traglia, F., Bonaccorso, A., Casagli, N. and Cristaldi, A. (2016): Monitoring crater-wall collapse at active volcanoes: a study of the 12 January 2013 event at Stromboli, *Bull. Volcanol.*, **78**(5), 39.

[7] Mori, T., and M. Burton (2009): Quantification of the gas mass emitted during single explosions on Stromboli with the $SO_2$ imaging camera, *J. Volcanol. Geotherm. Res.*, **188**(4), 395–400.

[8] Barnie, T., M. Bombrun, M. R. Burton, A. Harris, and G. Sawyer (2015): Quantification of gas and solid emissions during Strombolian explosions using simultaneous sulphur dioxide and infrared camera observations, *J. Volcanol. Geotherm. Res.*, **300**(0), 167–174.

**Telops Inc.**
100-2600 St-Jean Baptiste Ave
Québec, QC, Canada, G2E 6J5

+1-418-864-7808
sales@telops.com
www.telops.com